Accurate prediction of shape and size of polyvinyl alcohol beads produced by extrusion dripping

Mario Ignacio Weibel, Luciano Nicolás Mengatto, Julio Alberto Luna & Ignacio Rintoul

Iranian Polymer Journal

ISSN 1026-1265
Volume 27
Number 3

Iran Polym J (2018) 27:161-170
DOI 10.1007/s13726-017-0597-y

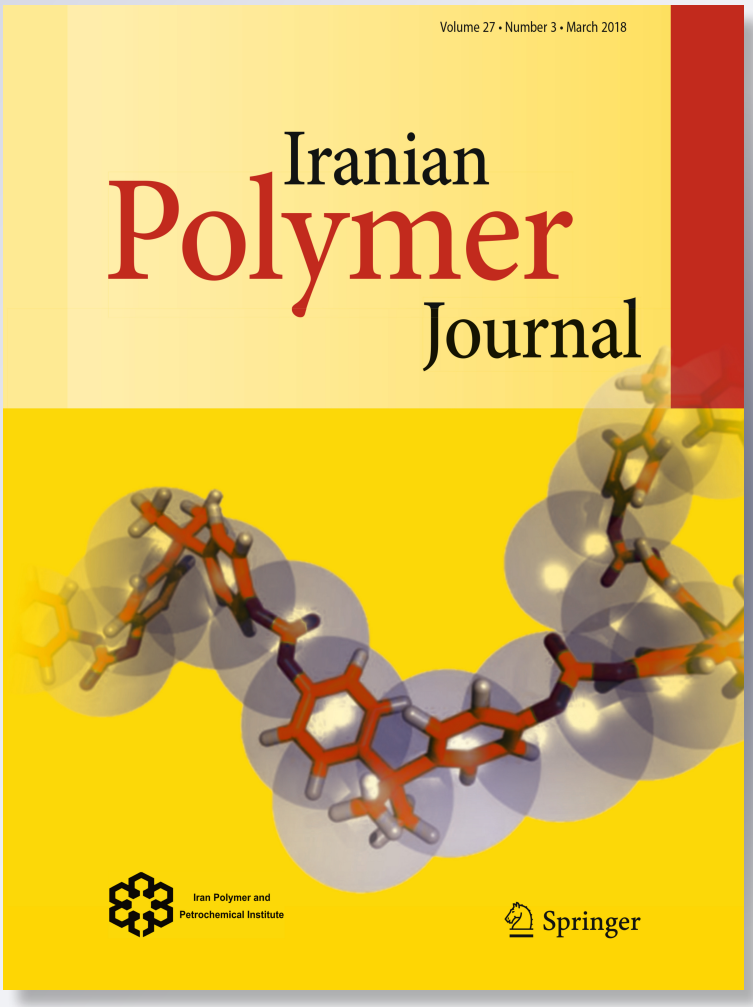

Springer

Iranian Polymer Journal (2018) 27:161–170
https://doi.org/10.1007/s13726-017-0597-y

ORIGINAL RESEARCH

Accurate prediction of shape and size of polyvinyl alcohol beads produced by extrusion dripping

Mario Ignacio Weibel[1] · Luciano Nicolás Mengatto[1] · Julio Alberto Luna[1] · Ignacio Rintoul[1]

Received: 7 July 2017 / Accepted: 26 December 2017 / Published online: 17 January 2018

Abstract

Beads are one of the particulate delivery systems used to achieve protection and/or controlled delivery of different active ingredients or microorganisms. Polyvinyl alcohol is a non-toxic and biodegradable polymer and possesses extensive applications as a biomaterial. In the present work, two different strategies were applied for the prediction of shape and size of polyvinyl alcohol beads. These beads were obtained by extrusion dripping of a boric acid–polyvinyl alcohol aqueous solution into a basic aqueous gelling bath. The shapes and sizes of immature, mature and dry beads were determined using optical microscopy. Two different strategies included statistical and fluid dynamical (mechanistic) models to fit the experimental data. The shape of immature and mature beads was found to be dependent on the viscosity of the dripping solution for the former and the maturation time for the latter. The shape of dry beads was found to be mainly dependent on the particle contraction in the drying process. The size of mature and dried beads was correctly predicted from the operating conditions by means of a statistically developed model and from the dripping solution properties by means of a fluid dynamical approach. The optimal conditions for minimal dried bead size were calculated. The obtained mathematical models allow reduction in the amount of resources and time taken in the initial stages of the development of a novel encapsulated formulation. The mechanistic model may be applied to other polymeric systems once the corresponding parameters have been determined during proof-of-concept experiments.

Keywords Beads · Extrusion dripping · Modelling · Polyvinyl alcohol (PVA) · Shape · Size

List of symbols

$[H_3BO_3/PVA]$	Boric acid to polyvinyl alcohol ratio, g H_3BO_3/100 g PVA
[PVA]	Polyvinyl alcohol concentration, %
A_b	Area of the bead, mm^2
d_b	Equivalent diameter, mm
$d_{b,d}$	Dried bead diameter, mm
$d_{b,i}$	Immature bead diameter, mm
$d_{b,m}$	Mature bead diameter, mm
$d_{b,t}$	Bead diameter as obtained from Tate's Law, mm
d_{max}	Length of perpendicular major axis, mm
d_{min}	Length of perpendicular minor axis, mm
d_o	Outer needle diameter, mm
F_{HB}	Harkins–Brown factor
$F_{HB}^{H_2O}$	Harkins–Brown factor for distilled water
F_{HB}^{sn}	Harkins–Brown factor for polymeric solution
g	Gravity constant
h	Distance of flight, cm
K_D	Drying factor
K_{LF}	Liquid lost factor
K_{SF}	Shrinkage factor
m_{H_2O}	Weight of a certain number of distilled water drops, g
m_{sn}	Weight of a certain number of polymer solution drops, g
Oh	Ohnesorge number
SF	Sphericity factor
$SF_{b,d}$	Dried bead sphericity factor

Electronic supplementary material The online version of this article (https://doi.org/10.1007/s13726-017-0597-y) contains supplementary material, which is available to authorized users.

✉ Mario Ignacio Weibel
marioweibel@gmail.com

[1] Instituto de Desarrollo Tecnológico para la Industria Química (INTEC), Universidad Nacional del Litoral (UNL), Consejo Nacional de Investigaciones Científicas y Técnicas (CONICET), Colectora Ruta Nacional 168, Paraje El Pozo, 3000 Santa Fe, Argentina

$SF_{b,i}$	Immature bead sphericity factor
$SF_{b,m}$	Mature bead sphericity factor
V_{ideal}	Ideal volume of a drop detaching from the tip of a needle, mm^3
V_{real}	Real volume of a drop detaching from the tip of a needle, mm^3
μ_{sn}	Viscosity of the polymeric solution, cP
ρ_{sn}	Density of the polymeric solution, kg/m^3
σ_{H_2O}	Surface tension of bidistilled water, mN/m
σ_{sn}	Surface tension of the polymeric solution, mN/m

Introduction

Encapsulation is a process by which an active ingredient or compound is trapped or confined inside a matrix or surrounded by a protective shell. The purpose of this process is to achieve one or more of the following objectives: immobilization [1], protection [2], stabilization [3] and/or controlled release [4] of the encapsulated active ingredients. Since the first application of encapsulation in carbonless copy paper in 1951, it has been applied to diverse fields including pharmaceutics, food, cosmetics, textile, biomedicine, electronics and agriculture [5]. Controlled release properties of the encapsulated active ingredient are particularly affected by particles size and shape [6]. In general, monodisperse and spherical particles are preferred due to the advantages in control of the release rate, free flow during handling and storage and aesthetics. Spherical beads with narrow size distributions can be easily obtained through employing optimized extrusion-dripping techniques [7].

Polyvinyl alcohol (PVA) is an important synthetic polymer obtained by transesterification of polyvinyl acetate with methanol in the presence of sodium hydroxide (NaOH). It is a highly hydrophilic, biodegradable and low-cost material approved by the United States Food and Drug Administration (FDA) for its use in medicine [8, 9]. Its main property, solubility in water, depends on hydrolysis and polymerization degree and temperature [10]. PVA hydrogels have been used in the controlled release of different active substances such as analgesics [11], antibiotics [11], anticancer drugs [12], vasoactive drugs [13], proteins [14], nanoparticles [15] and anti-corrosion products [16]. Furthermore, PVA can be cross-linked by chemical procedures using glutaraldehyde, polycarboxylic acids, or boric acid (H_3BO_3) in a basic medium [10]. In particular, a method has been reported to produce PVA beads with narrow size distributions and uniform shape by extruding a H_3BO_3–PVA aqueous solution through a nozzle [17]. The solution drops at a controlled rate into a gelling bath with basic pH. Then, the cross-linking reaction between H_3BO_3 and PVA takes place and beads are formed in a sol–gel transition. A two-step reaction was proposed. First, a mono-diol structure was formed because of the reaction between a 1,3-diol unit of PVA with a borate ion. In the second stage, this mono-diol moiety reacted with another 1,3-diol unit of PVA, leading to the formation of a network with inter- and intra-molecular cross-linking [18]. The nature of this cross-linking could be ionic or covalent and it is still under discussion [19]. Even though this method has several applications in controlled release of drugs, other versions have been recently applied to the immobilization of bacteria [20], catalysts [21] and enzymes [22].

Several parameters including particle/shell material, active ingredient concentration, density, viscosity and surface tension of the dripping and gelling solution, dripping speed, needle size and flight distance can influence the final size and shape of the resulting beads [23]. Therefore, a great amount of trial-and-error work is needed to find the optimal conditions for a required particle size and shape. This issue represents the major constraint when studying and scaling up a new microencapsulation process. To overcome this problem, a semi-empirical model has been developed to introduce several correction factors to Tate's Law to predict the size of alginate beads produced by extrusion dripping accurately [24]. This model has also been applied recently to the production of chitosan–alginate [25], xanthan gum–alginate [26] and pectinate [27] capsules with good success. Other mathematical models were also developed for alginate beads production by air extrusion [28], jet cutting [29] and ultrasonic atomization [30] methods. However, no efforts have been made to apply these mathematical models to the prediction of the shape and size of the PVA beads. Therefore, in this work, we assume the challenge applying two different strategies to develop mathematical models that allow reducing the time and resources employed in future research in encapsulation processes.

In this context, previous experiments showed that polymer concentration ([PVA]), cross-linker/polymer ratio ($[H_3BO_3/PVA]$), outer needle diameter (d_o) and flight distance (h) are four important factors affecting particle properties. In the present work, to avoid a trial-and-error work method, experimental design and rigorous modelling were employed. Different experiments were carried out to evaluate the size and shape of immature, mature and dried beads. The results of the experiments were analysed in two different ways. First, a statistical model was developed with the help of analysis of variance using statistical software. Secondly, a semi-empirical mechanistic model was developed. The applicability of both models has been studied and discussed. An operating window is accurately established and the optimal conditions for minimal dried bead size are obtained.

Experimental

Materials

Technical-grade PVA (Serquim, Argentina) with a hydrolysis degree of 88.3% and a viscosity of 48.6 cP (for a 4% solution in distilled water) was used as received. Its volatile content was considered in the preparation of solutions. Analytical-grade sodium chloride (NaCl) and NaOH (Laboratorios Cicarelli, Argentina) were used to adjust the ionic strength and the pH of the gelling bath. H_3BO_3 (Laboratorios Cicarelli, Argentina) was employed to adjust the cross-linking degree of the beads. Technical-grade type I B hydrolysed gelatine (PB Leiner, Argentina) was used to adjust the surface tension of the gelling bath. Type I B gelatine is an alkaline-conditioned gelatine derived from beef skin collagen. Double-distilled water was used in the preparation of solutions.

Measurement of the polymer solution properties

The density of the polymer solutions (ρ_{sn}) was determined using a 50.0 mL volumetric flask and an analytical balance with 0.1 mg resolution (Precisa Gravimetrics, Switzerland). The viscosity of the polymer solutions (μ_{sn}) was measured using a rotatory viscometer (Cannon Instrument Company, model 2020, USA). The standard procedure establishes the use of a 600 mL beaker with a 500 mL working volume, or an adapter for small sample volumes (UL Adapter Kit, Cannon Instrument Company, USA).

The surface tension of the polymer solutions (σ_{sn}) was determined gravimetrically by a drop weight-based method [31]. Each H_3BO_3–PVA solution was put in a 5 mL plastic syringe (Rymco, Colombia) with Luer-Lock connectors and extruded through a 21 G stainless steel needle (BD, USA) with its tip flattened, using a syringe pump (KD Scientific 200, USA) set at 1 mL/h flow rate. The weight of 20 drops was measured in each experiment. Double-distilled water was used as reference material. The experimental value of σ_{sn} was calculated using Eq. 1 [31]:

$$\sigma_{sn} = \sigma_{H_2O} \frac{m_{sn} F_{HB}^{H_2O}}{m_{H_2O} F_{HB}^{sn}}, \tag{1}$$

where m_{sn} and F_{HB}^{sn} are the drops' weight and the Harkins–Brown factor for the H_3BO_3–PVA solution and σ_{H_2O}, m_{H_2O} and $F_{HB}^{H_2O}$ are the surface tension, the drops' weight and the Harkins–Brown factor of double-distilled water, respectively. The Harkins–Brown factor is conceptually defined as the ratio between the real volume (V_{real}) and the ideal volume (V_{ideal}) of a drop detaching from the tip of a needle. The Harkins–Brown factor was obtained using the Lee–Chan–Pogaku (LCP) method, which its mathematical expression is shown in Eq. 2 [31]:

$$F_{HB} = 1.000 - 0.9121\frac{d_o/2}{V_{real}^{1/3}} - 2.109\left(\frac{d_o/2}{V_{real}^{1/3}}\right)^2 + 13.38\left(\frac{d_o/2}{V_{real}^{1/3}}\right)^3 - 27.29\left(\frac{d_o/2}{V_{real}^{1/3}}\right)^4 + 27.53\left(\frac{d_o/2}{V_{real}^{1/3}}\right)^5 - 13.58\left(\frac{d_o/2}{V_{real}^{1/3}}\right)^6 + 2.593\left(\frac{d_o/2}{V_{real}^{1/3}}\right)^7, \tag{2}$$

where ρ_{sn}, μ_{sn} and σ_{sn} were determined in 22–23 °C.

H_3BO_3–PVA bead production

The experimental part was carried out according to a well-established procedure [17]. Figure 1 shows a scheme of the bead preparation and the main factors involved in their synthesis. Polymer solutions were prepared by dissolving appropriate quantities of PVA in double-distilled water at 80–90 °C, under gentle stirring, for 1 h. Subsequently, different amounts of H_3BO_3 were dissolved in the PVA solution. Four polymer concentrations, [PVA] = 9, 7, 5 and 4% and three cross-linker/polymer ratios, [H_3BO_3/PVA] = 5.0, 7.5 and 10.0%, were studied. The gelling bath was prepared by dissolving 0.19 g NaOH and 6.9 g NaCl in double-distilled water up to 150 g of final solution weight. Afterwards, 2.5 g of gelatine was added to the bath to adjust its surface tension.

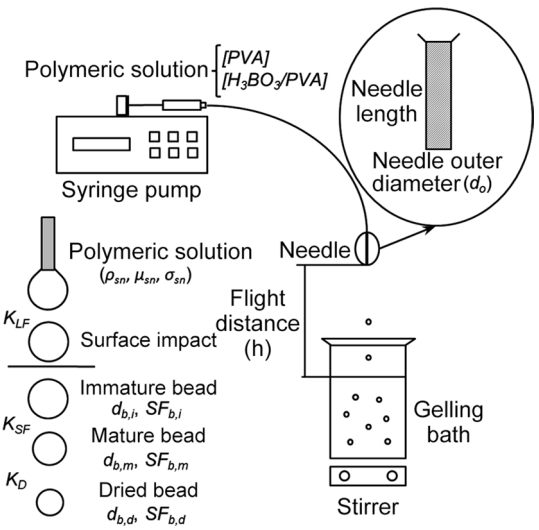

Fig. 1 Scheme of the H_3BO_3–PVA bead production and major parameters involved in their synthesis

The composition of the gelling bath was the same for all the experiments. All solutions were prepared before use.

The extrusion-dripping experiments were carried out in 22–23 °C. The 21 G, 19 G and 18 G stainless steel hypodermic needles (BD, USA) were used with their tips flattened and the length adjusted to 3 cm. The flight distance (h) was set at 6, 12 and 18 cm.

The PVA solutions were passed through the needle using a syringe pump (KD Scientific 200, USA) equipped with a 5 mL plastic syringe (Rymco, Colombia) with Luer-Lock connectors. Dripping flow was fixed at 1 mL/h to exclude any kinematic effect inherent to flow forces.

The samples of immature and mature beads were collected from the gelling bath immediately after drop impact and after a hardening time of 60 min, respectively. By completion of this time period, all the remaining beads were filtered, washed twice with double-distilled water and finally dried in warm air stream ($T < 40$ °C). They were kept in movement during all the process to avoid agglomeration. Finally, they were vacuum dried and stored in a desiccator until characterization.

Shape and size analysis of immature, mature and dried beads

Samples of immature, mature and dried beads were examined under an optical microscope (Leica DM 2500 M, Germany) equipped with a high-resolution digital camera (Leica DFC290 HD, Germany). Images were processed and bead dimensions were determined using ImageTool 3.0 software (University of Texas Health Science Center at San Antonio, USA). Bead area (A_b) and maximum (d_{max}) and minimum (d_{min}) perpendicular diameters were obtained. The equivalent diameter (d_b) was selected as the bead size parameter and calculated according to Eq. 3 for immature ($d_{b,i}$), mature ($d_{b,m}$) and dried ($d_{b,d}$) beads:

$$d_b = \sqrt{\frac{4A_b}{\pi}}. \tag{3}$$

The sphericity factor (SF) was calculated according to Eq. 4 [24]. SF is a sensible dimensionless shape factor adopted to describe the bead shape deviation from a perfect sphere [24]. For a perfect sphere, the SF is equal to zero. However, a bead can be considered to be practically spherical if SF < 0.05 [24].

$$\mathrm{SF} = \frac{d_{max} - d_{min}}{d_{max} + d_{min}}. \tag{4}$$

Immature ($SF_{b,i}$), mature ($SF_{b,m}$) and dried bead ($SF_{b,d}$) sphericity factors were determined, accordingly.

The Ohnesorge number (Oh) in Eq. 5 is a dimensionless parameter that compares viscous and surface tension forces taking place in dripping phenomena. This parameter was calculated for each type of bead and used in the analysis of bead shape:

$$Oh = \frac{\mu_{sn}}{\sqrt{\rho_{sn} d_{b,i} \sigma_{sn}}}. \tag{5}$$

The fluid dynamical approach for the bead size prediction was developed according to a model elaborated for shape and size prediction of alginate beads produced by extrusion dripping [22]. Briefly, the model predicts $d_{b,m}$ using Eq. 6 as follows:

$$d_{b,m} = K_{LF} K_{SF} d_{b,i}, \tag{6}$$

Here, $d_{b,t}$ is the theoretical bead diameter as obtained by the Tate's Law according to Eq. 7:

$$d_{b,t} = \sqrt[3]{\frac{6000 d_o \sigma_{sn}}{\rho_{sn} g}}, \tag{7}$$

where g is the gravitational constant.

K_{LF} is defined according to Eq. 8:

$$K_{LF} = \sqrt[3]{\frac{V_{real}}{V_{ideal}}} = \sqrt[3]{F_{HB}}. \tag{8}$$

K_{SF} is determined according to Eq. 9. This factor includes the loss of water during shrinkage of the bead due to high saline concentration of the gelling bath and the cross-linking process:

$$K_{SF} = \frac{d_{b,m}}{d_{b,i}}. \tag{9}$$

A drying factor (K_D) was also introduced to explain the contraction observed during drying and was estimated as in Eq. 10:

$$K_D = \frac{d_{b,d}}{d_{b,m}}. \tag{10}$$

The statistical study of mature beads size ($d_{b,m}$) was done by applying several models contained in Design-Expert software 8.0.7.1 Trial Version (Stat-Ease Inc., USA). Only those experiments that fit a 3^4 full factorial design are taken into account in the analysis and correspond to the experiments from #1 to #81 listed in Online Resource (Table S1).

Due to agglomeration, the size of dried beads ($d_{b,d}$) could only be analysed statistically by fitting the experimentally available data into linear models with the use of the free software R 2.15.1 version (The R Foundation for Statistical Computing, Austria).

Results and discussion

For the purposes of the current work, this section is organized as follows. The results obtained in the measurement of the physicochemical properties of the H_3BO_3–PVA solutions are described in "Properties of the polymer solutions". "H_3BO_3–PVA beads production" includes some important comments about the synthesis of the polymeric beads. In "Shape and size analysis of immature, mature and dried beads", the analysis of bead shape as a function of the *Oh* number and the analysis of bead size are described employing two different strategies, a fluid dynamical (mechanistic) model and a statistical approach. The section under "optimization" describes the procedure to determine the best conditions to minimize beads.

Properties of polymeric solutions

The experimental values for ρ_{sn} ranged from 1007 (for [PVA] = 4% and [H_3BO_3/PVA] = 5%) to 1022 kg/m^3 (for [PVA] = 9% and [H_3BO_3/PVA] = 10%), with the reference value for double-distilled water equal to 997 kg/m^3. A slight increase in ρ_{sn} was observed when [PVA] increased. Minor variations in ρ_{sn} were also measured when [H_3BO_3/PVA] was modified.

The values of σ_{sn} ranged between 51.1 and 52.8 mN/m. The σ_{sn} values obtained for the polymer solutions were lower than the σ_{sn} reference value of double-distilled water (72.6 mN/m) and were unaffected by the modification of [PVA] and [H_3BO_3/PVA]. This result was in agreement with literature. It has been reported that, independently of the polymerization degree of PVA, the decrease of surface tension as a function of polymer concentration is reduced when PVA concentration is higher than 0.25%. This is due to a lower attraction of the water molecules on the surface by PVA molecules inside the solution [32]. Therefore, the surface of the liquid can be considered as a surface saturated with the molecules of PVA. Low surface tension values are desired during the drop formation process.

Generally, polymer solutions present a non-Newtonian fluid rheological behaviour. Particularly, PVA aqueous solutions are considered as shear thickening materials, showing a viscosity increment when the shear rate is raised. However, in small ranges of shear rates, PVA aqueous solutions can be considered as Newtonian fluids [33]. In the experiments carried out in the present work, the applied shear rate was in the range of 0.7–22 s^{-1} and could be considered low enough to ensure the Newtonian behaviour for the polymer solutions. The measured μ_{sn} values ranged from 48 (for [PVA] = 4% and [H_3BO_3/PVA] = 5%) to 5136 cP (for [PVA] = 9% and [H_3BO_3/PVA] = 10%) were strongly influenced by [PVA] and [H_3BO_3/PVA].

Polyvinyl alcohol concentration is a known thickener due to its inter- and intra-molecular interactions generated by hydrogen bonds between pendant hydroxyl groups. As [PVA] grows, the distances between the chains become shorter and the motion of molecule segments is hindered. In the same way, the incorporation of borate mono-diol structures through the PVA chains may reduce the segment mobility and hinder the flux. Detailed experimental values for ρ_{sn}, σ_{sn} and μ_{sn} are presented in Online Resource (Table S2 and Table S3).

About the H_3BO_3–PVA bead production

A total of 108 experiments were carried out (Online Resource, Table S1) and, in all of them, immature and mature beads were obtained. Cross-linking reaction and sol–gel transition were assured by maintaining the pH above 10, with the presence of NaOH in the gelling bath. According to literature, this condition permits the formation of a network and the sudden increase in viscosity that leads to the sol–gel transition [34].

Nevertheless, not all the conditions resulted in the production of individual dried beads; thus the number of experiments used in the analysis of dried bead data was limited. A possible explanation for this behaviour is related to the loss of PVA dissolved in water during drying. This PVA might come from a possible incomplete formation of the three-dimensional network at low values of [PVA] [35]. The known adhesive properties of PVA finally caused the agglomeration between beads for the experiments with [PVA] = 4% and all [H_3BO_3/PVA] levels, and [PVA] = 5% and [H_3BO_3/PVA] = 5%.

Shape and size analysis of immature, mature and dried beads

Figure 2 shows $SF_{b,i}$ as a function of the Ohnesorge number. The values obtained for *Oh* are between 0.1 and 13.4. When *Oh* takes extreme values, $SF_{b,i}$ values are higher than 0.05 and the beads differ from the spherical shape. Since σ_{sn} and ρ_{sn} are approximately constant, the variation of *Oh* with [PVA] and [H_3BO_3/PVA] can be assigned almost exclusively to the variation of μ_{sn}. Polymer solutions with *Oh* values between 0.1 and 3 have resulted in beads with $SF_{b,i}$ lower than 0.05. This corresponds to 40 cP < μ_{sn} < 1200 cP. When a drop hits the surface of the gelling bath, an equilibrium of forces takes place: viscous and surface tension forces of the drop act against the impact inertial and drag forces of the gelling bath. The use of hydrolysed beef gelatine decreased the surface tension and reduced the impact strength of the surface of the gelling bath.

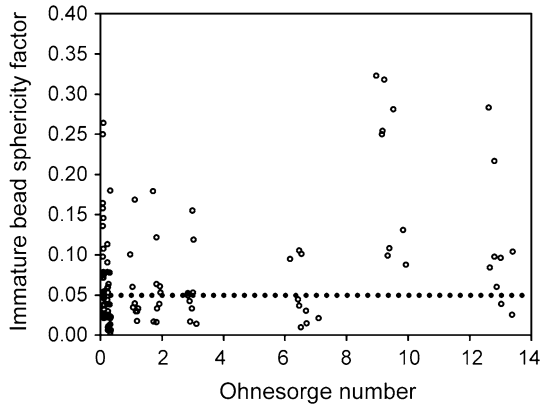

Fig. 2 Variation of immature bead sphericity factor as a function of the Ohnesorge number

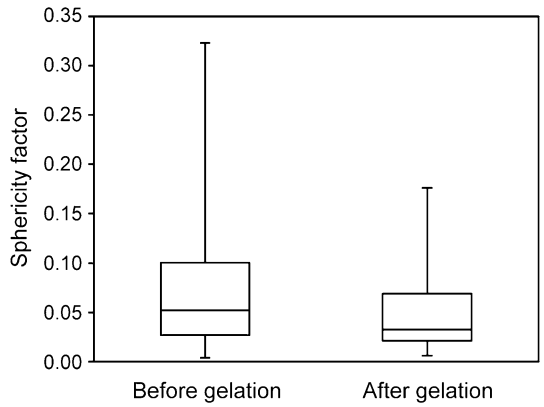

Fig. 3 Box-and-whisker diagram distribution of sphericity factor values, before (immature beads) and after (mature beads) gelation

Polymer solutions at [PVA] < 4% and with low *Oh* presented very low viscosity to overcome the impact of the surface and the obtained drops deviated from the spherical shape. Polymer solutions at [PVA] < 9% and with high *Oh* developed a bridge of polymer between the falling drop and the needle tip. This effect ultimately resulted in pear- or tear-shaped beads and established the upper viscosity limit of the extrusion-dripping process. This result was also reported for alginate systems [36]. Figure 3 shows the effect of the 60 min maturation time on the SF values and Fig. 4 presents an example of immature, mature and dried bead shape.

Shapiro–Francia test showed that the sample distributions were not normal ($p < 0.05$). Wilcoxon test for paired samples showed that the population means differed significantly ($p < 0.05$). The maturation time allowed polymer chains to relax and the beads to take a spherical shape to minimize their acting surface forces. This effect reduced the data dispersion. Interestingly, the average $SF_{b,d}$ was higher than $SF_{b,m}$. This can be explained by the contraction generated during drying, which makes the beads adopt irregular shapes.

Figure 5 presents images from selected samples showing the size monodispersity and the irregular shape of the dried beads.

For the fluid dynamical analysis of bead sizes, the full set of experiments was used to determine K_{LF}, K_{SF} and K_D. K_{LF} was obtained by a semi-empirical method using experimentally determined V_{real}, Eq. 2 and the second equality of Eq. 8. As described in Ref. [24], K_{LF} could be better correlated with d_o to obtain a simpler mathematical expression. The linear fitting ($R^2 = 0.94$) is expressed in Eq. 11:

$$K_{LF} = 0.9745 - 0.0499 d_o. \quad (11)$$

K_{SF} was calculated experimentally by measuring $d_{b,i}$ and $d_{b,m}$. Neither a linear model nor the mean made a good prediction of the data. Furthermore, due to the left skewed asymmetric distribution of K_{SF}, the median was a better estimate than the arithmetic mean to represent the population and was 0.833.

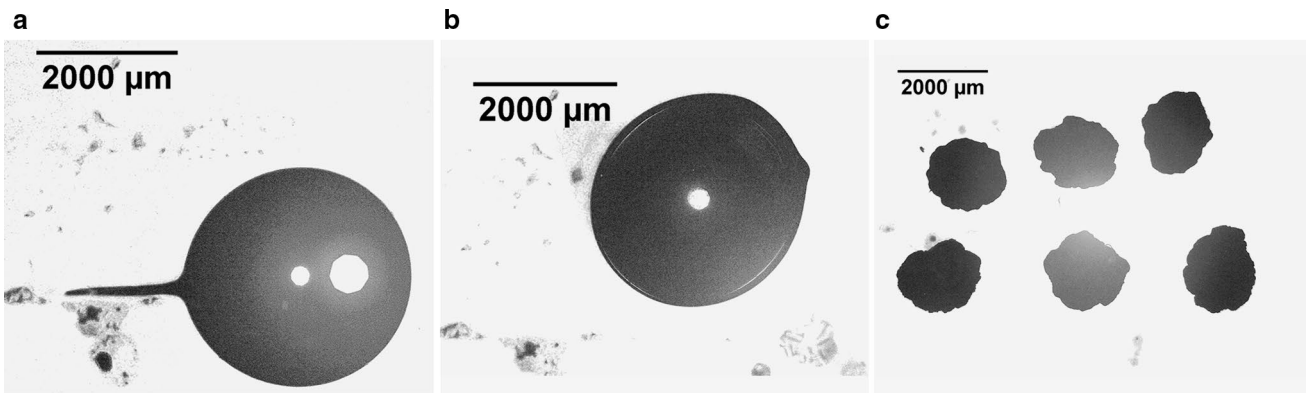

Fig. 4 Effect of the maturation time on the bead shape corresponding to the following parameters: [PVA] = 9%, [H_3BO_3/PVA] = 7.5%, d_o = 1.2700 mm and h = 6 cm: **a** immature bead, **b** mature bead and **c** dried bead

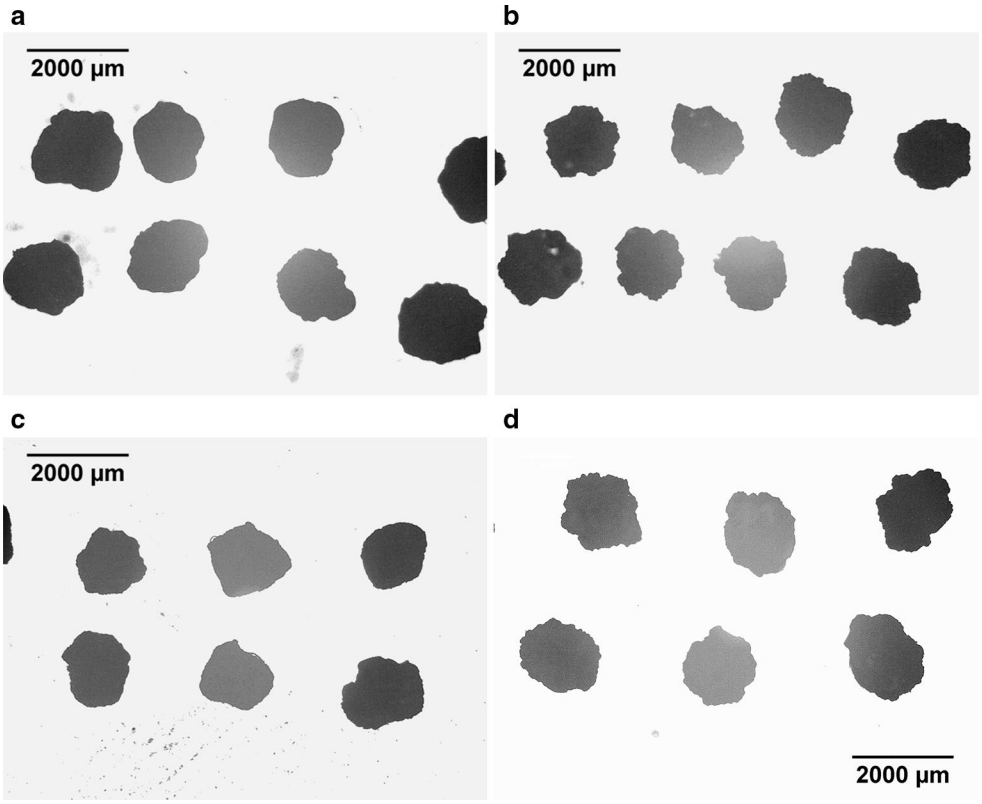

Fig. 5 Images from selected dried bead samples corresponding to the following experiences: **a** [PVA] = 9%, [H_3BO_3/PVA] = 7.5%, d_o = 0.8192 mm and h = 6 cm, **b** [PVA] = 7%, [H_3BO_3/PVA] = 7.5%, d_o = 0.8912 mm and h = 6 cm, **c** [PVA] = 5%, [H_3BO_3/PVA] = 7.5%, d_o = 0.8912 mm and h = 6 cm (optimal conditions), **d** [PVA] = 5%, [H_3BO_3/PVA] = 7.5%, d_o = 1.2700 mm and h = 6 cm

The fluid dynamical model obtained for the mature bead size is presented in Eq. 12:

$$d_{b,m} = K_{SF}K_{LF}d_{b,t} = \left(0.860 - 0.044d_o\right)\sqrt[3]{\frac{6000d_o\sigma_{sn}}{\rho_{sn}g}}. \quad (12)$$

This mathematical expression predicts the mature bead diameter obtained by extrusion dripping of a H_3BO_3–PVA solution as a function of the polymer solution properties and outer needle diameter. Figure 6a shows the adjustment between the experimental and predicted data. A negative deviation is observed with maximum and mean absolute deviations of 18.8 and 4.1%, respectively.

As mentioned above, during drying, agglomeration was observed in the beads produced at [PVA] = 4 and 5% and [H_3BO_3/PVA] = 5%. These experiments were excluded for subsequent analysis of dried bead size. Consequently, the number of valid experiments was reduced from 108 to 76. When applicable, K_D was calculated experimentally by measuring $d_{b,d}$ and $d_{b,m}$. The arithmetic mean for K_D was 0.568. Equation 13 presents the model to predict $d_{b,d}$. The maximum and mean absolute deviations were 16.7 and 5.5%. Figure 6b shows the adjustment between the experimental and predicted data.

$$d_{b,d} = 0.568(0.860 - 0.044d_o)\sqrt[3]{\frac{6000d_o\sigma_{sn}}{\rho_{sn}g}}. \quad (13)$$

For the statistical analysis of bead size, the main effects and interactions on $d_{b,m}$ were determined using a 3^4 full factorial experimental design with four factors, [PVA], [H_3BO_3/PVA], d_o and h, at three levels. This corresponds to the first 81 experiments listed in Online Resource (Table S1). Table 1 shows the results from the ANOVA. A quadratic model describes data and its probability value is smaller than 0.05, indicating that the model terms are significant. Significant model terms ($p < 0.05$, Table 1) were used to obtain the final expression of the model according to Eq. 14:

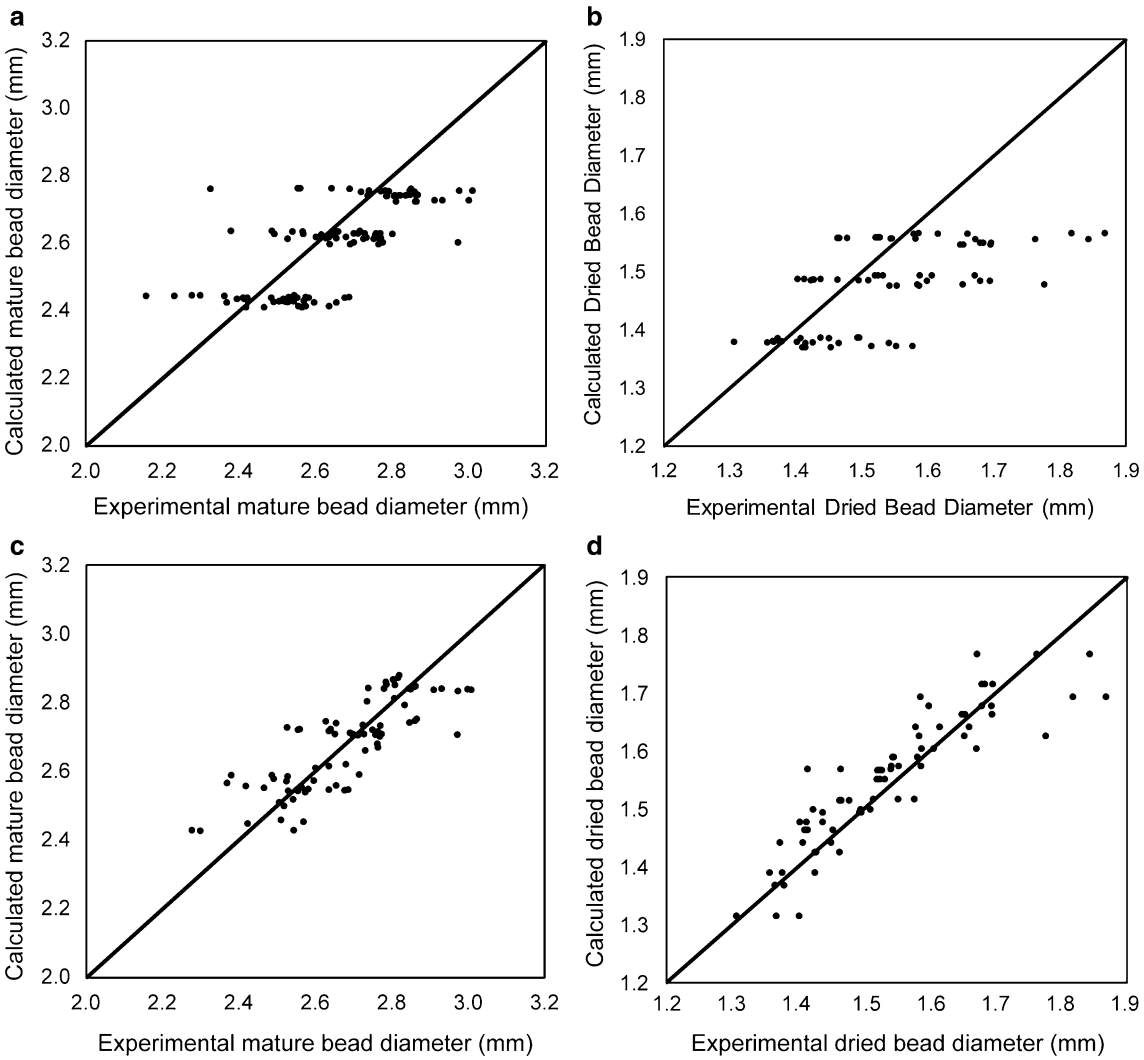

Fig. 6 Correlation between experimental and calculated beads size data: **a** fluid dynamical analysis for mature beads, **b** fluid dynamical analysis for dried beads, **c** statistical analysis for mature beads and **d** statistical analysis for dried beads

$$d_{b,m} = 1.1165 + 0.2256[PVA] + 0.6515d_o - 4.647 \times 10^{-3}[PVA][H_3BO_3/PVA] - 3.009 \times 10^{-4}[PVA]h + 3.216.10^{-4}[H_3BO_3/PVA]h - 0.01173[PVA]^2 + 2.372.10^{-3}[H_3BO_3/PVA]^2. \quad (14)$$

The model presented a suitable adjusted $R^2 = 0.73$, indicating a good relationship between the experimental data and the fitted model and a low coefficient of variation of 3.1%. The maximum (8.9%) and mean (2.8%) absolute deviations were also low. Figure 6c shows a good agreement between the experimental results and predicted data.

A linear model, shown in Eq. 15, was found to be significant ($p < 0.05$) for the response $d_{b,d}$. This model has explained 81% of the data variability. Maximum and mean absolute deviations of 10.9 and 2.7% resulted. Figure 6d shows the adjustment between the experimental and predicted data.

$$d_{b,d} = 0.9771 + 0.03714[PVA] - 0.02084[H_3BO_3/PVA] + 0.4410d_o. \quad (15)$$

Optimization

As the bead shrinkage during drying was almost the same in all the experiments, $d_{b,d}$ was directly related with $d_{b,m}$, as seen from Eq. 13. Regarding the already discussed limitations during bead drying and considering the difficulty of

Table 1 ANOVA results for the response $d_{b,m}$

Source	*F* value	*p* value
Model	15.61	< 0.0001
[PVA]	15.29	0.0002*
[H_3BO_3/PVA]	3.38	0.0706
d_o	161.06	< 0.0001*
h	0.31	0.5798
[PVA] [H_3BO_3/PVA]	10.75	0.0017*
[PVA] d_o	0.59	0.4436
[PVA] h	4.35	0.0408*
[H_3BO_3/PVA]d_o	0.80	0.3738
[H_3BO_3/PVA]h	4.66	0.0346*
$d_o h$	0.02	0.8988
$[PVA]^2$	5.50	0.0221*
$[H_3BO_3/PVA]^2$	10.42	0.0019*
d_o^2	0.07	0.7975
h^2	0.05	0.8287

*Significance level $p < 0.05$

H_3BO_3 dissolution in the aqueous PVA solution, an optimization method to determine the minimum $d_{b,m}$ based on Eq. 12 was employed. Using the optimization package included in Design-Expert 8.0.7.1 Trial Version, the desirability function was maximized (0.919) for the following dripping conditions: [PVA] = 5%, [H_3BO_3/PVA] = 5%, 21G needle and h = 6 cm. In these particular conditions, the predicted and experimental values for $d_{b,m}$ were in good agreement and were 2.34 and 2.30 mm, respectively. However, in these experimental conditions, bead agglomeration was observed during drying. As [H_3BO_3/PVA] showed a minor effect on the bead size compared to [PVA], the optimal conditions could be redefined as: [PVA] = 5%, [H_3BO_3/PVA] = 7.5%, 21 G needle and h = 6 cm. The experimental values found for $d_{b,m}$ and $d_{b,d}$ in these particular conditions were 2.42 and 1.37 mm, respectively. For $d_{b,m}$, the values predicted by Eqs. 12 and 14 were 2.43 and 2.45 mm, respectively. For $d_{b,d}$, the values predicted by Eqs. 13 and 15 were 1.36 and 1.38 mm, respectively.

Conclusion

The proposed experimental design allowed determining the major factors involved in bead formation, and size and shape setting. The shape of immature beads was observed to depend mainly on the viscosity of the dripping polymer solution. In particular, *Oh* was an excellent dimensionless factor to study bead shape variation with the properties of the polymer solution. The optimal values of μ_{sn} to obtain spherical immature beads ranged from 40 to 1200 cP. The bead shape was also found to be affected by the maturation in the gelling bath, leading to a decrease in the value of SF. The conditions of the drying process also showed a major effect on the shape of dried beads.

Both modelling approaches studied in the present work were useful to accurately estimate the size of mature beads obtained in certain conditions. The fluid dynamical model allowed estimating mature bead size from the physicochemical properties of the polymer solution (density, viscosity and surface tension), while the statistical model could be used to estimate mature bead size from the operating conditions (polymer concentration, cross-linker/polymer ratio, needle diameter and flight distance). The selection of the proper model would depend on the data available prior to the experiment. In particular, the applicability of the mechanistic fluid dynamical model to several other extrusion-dripping processes employing different polymers (natural or synthetic) might be done once the parameters K_{SF} and K_{LF} have been determined for each specific system during proof-of-concept trials.

Future work should be based on two aspects: the possibility to consider more factors to those taken into account in this study (i.e. influence of gelling bath conditions, flow speed, etc.) and the extension of this model to the formation of drug-loaded beads.

Acknowledgements The authors thank the Consejo Nacional de Investigaciones Científicas y Técnicas and the Instituto de Promoción de la Carne Vacuna Argentina for their financial support.

Compliance with ethical standards

Conflict of interest The authors declare that they have no conflict of interest.

References

1. Dintcheva NT, Catalano G, Arrigo R, Morici E, Cavallaro G, Lazzara G, Bruno M (2016) Pluronic nanoparticles as anti-oxidant carriers for polymers. Polym Degrad Stab 134:194–201
2. Zhang Z, Zhang R, Chen L, Tong Q, McClements DJ (2015) Designing hydrogel particles for controlled release of targeted release of lipophilic bioactive agents in the gastrointestinal tract. Eur Polym J 72:698–716
3. He H, Hong Y, Gu Z, Liu G, Cheng L, Li Z (2016) Improved stability and controlled release of CLA with spray-dried microcapsules of OSA-modified starch and xanthan gum. Carbohydr Polym 147:243–250
4. Savoji MT, Zhu XX (2015) Temperature- and pH-controlled encapsulation and release of guest molecules from invertible carriers. Polymer 68:35–40
5. Martins IM, Barreiro MF, Coelho M, Rodrigues AE (2014) Microencapsulation of essential oils with biodegradable polymeric carriers for cosmetic applications. Chem Eng J 245:191–200
6. Mitragotri S, Burke PA, Langer R (2014) Overcoming the challenges in administering biopharmaceuticals: formulation and delivery strategies. Nat Rev Drug Discov 13:655–672

7. Heinzen C, Berger A, Marison I (2004) Use of vibration technology for jet break-up for encapsulation of cells and liquids in monodisperse microcapsules. In: Nedović V, Willaert R (eds) Fundamentals of cell immobilisation biotechnology. Springer, Dordrecht, pp 257–275
8. DeMerlis CC, Schoneker DR (2003) Review of the oral toxicity of polyvinyl alcohol (PVA). Food Chem Toxicol 41:319–326
9. Baker MI, Walsh SP, Schwartz Z, Boyan BD (2012) A review of polyvinyl alcohol and its uses in cartilage and orthopedic applications. J Biomed Mater Res, Part B 100B:1451–1457
10. Hassan CM, Peppas NA (2000) Structure and applications of poly(vinyl alcohol) hydrogels produced by conventional crosslinking or by freezing/thawing methods. Biopolymers PVA Hydrogels, Anionic Polymerisation Nanocomposites. Springer Verlag, Berlin, pp 37–65
11. Anirudhan TS, Parvathy J, Nair AS (2016) A novel composite matrix based on polymeric micelle and hydrogel as drug carrier for the controlled release of dual drugs. Carbohydr Polym 136:1118–1127
12. Chang G, Chen Y, Li Y, Huang F, Shen Y, Xie A (2015) Self-healable hydrogel on tumor cell as drug delivery system for localized and effective therapy. Carbohydr Polym 122:336–342
13. Kaity S, Isaac J, Ghosh A (2013) Interpenetrating polymer network of locust beam gum-poly (vinylalcohol) for controlled release drug delivery. Carbohydr Polym 94:456–467
14. Luo Y, Luo G, Gelinsky M, Huang P, Ruan C (2017) 3D bioprinting scaffold using alginate/polyvinyl alcohol bioinks. Mater Lett 189:295–298
15. Yan E, Fan S, Li X, Wang C, Sun Z, Ni L, Zhang D (2013) Electrospun polyvinyl alcohol/chitosan composite nanofibers involving Au nanoparticles and their in vitro release properties. Mater Sci Eng C 33:461–465
16. Gu T, Liu X, Chai W, Li B, Sun H (2014) A preliminary research on polyvinyl alcohol hydrogel: a slowly-released anti-corrosion and scale inhibitor. J Pet Sci Eng 122:453–457
17. Rintoul I, Badano JM, Grau R (2014) Controlled-release injectable microparticle. USPatent 20140335193:A1
18. Ochiai H, Shimizu S, Tadokoro Y, Murakami I (1981) Complex formation between poly(vinyl alcohol) and borate ion. Polymer 22:1456–1458
19. Shibayama M, Yoshizawa H, Kurokawa H, Fujiwara H, Nomura S (1988) Sol-gel transition of poly(vinyl alcohol)-borate complex. Polymer 29:2066–2071
20. Jeong D, Cho K, Lee CH, Lee S, Bae H (2016) Integration of forward osmosis process and continuous airlift nitrifying bioreactor containing PVA/alginate-immobilized beads. Chem Eng J 306:1212–1222
21. Rahman AHA, Teo CL, Idris A, Misran E, Leong SAN (2016) Polyvinyl alcohol-alginate ferrophoto gels for mercury(II) removal. J Ind Eng Chem 33:190–196
22. Seker DC, Zain NAM (2014) Response surface optimization of glucose production from liquid pineapple waste using immobilized invertase in PVA-alginate-sulfate beads. Sep Purif Technol 133:48–54
23. Lee BB, Ravindra P, Chan ES (2013) Size and shape of calcium alginate beads produced by extrusion dripping. Chem Eng Technol 36:1627–1642
24. Chan ES, Lee BB, Ravindra P, Poncelet D (2009) Prediction models for shape and size of ca-alginate macrobeads produced through extrusion-dripping method. J Colloid Interface Sci 338:63–72
25. Lim GP, Lee BB, Ahmad MS, Singh H, Ravindra P (2016) Influence of process variables and formulation composition of sphericity and diameter of Ca-alginate-chitosan liquid core capsules prepared by extrusion dripping method. Part Sci Technol 34:681–690
26. Ong HY, Lee BB, Zakaria Z, Chang ES (2015) Diameter prediction mathematical models for xanthan gum-alginate capsules produced by extrusion-dripping method. In: AIP Conf Proc, vol 1660, pp 070034(1–6)
27. Lee BB, Chan ES, Ravindra P (2014) Calcium pectinate beads formation: shape and size analysis. J Eng Technol Sci 46:78–92
28. Lee BB, Bhandari BR, Howes T (2016) Air extrusion system for ionotropic alginate microgel particles formation: a review. Chem Eng Technol 39:2355–2369
29. Paulo BB, Ramos FM, Prata AS (2017) An investigation of operational parameters of jet cutting method on the size of Ca-alginate beads. J Food Process Eng 40:e12591. https://doi.org/10.1111/jfpe.12591
30. Dalmoro A, Barba AA, d'Amore M (2013) Analysis of size correlations for microdroplets produced by ultrasonic atomization. World Sci J 2013:1–7 **(ID482910)**
31. Lee BB, Ravindra P, Chan ES (2009) New drop weight analysis for surface tension determination of liquids. Colloids Surf A 332:112–120
32. Bhattacharya A, Ray P (2004) Studies on surface tension of poly(vinyl alcohol): effect of concentration, temperature, and addition of chaotropic agents. J Appl Polym Sci 93:122–130
33. Rošic R, Pelipenko J, Kristl J, Kocbek P, Bešter-Rogač M, Baumgartner S (2013) Physical characteristics of poly (vinyl alcohol) solutions in relation to electrospun nanofiber formation. Eur Polym J 49:290–298
34. Shibayama M, Sato M, Kimura Y, Fujiwara H, Nomura S (1988) ^{11}B n.m.r. study on the reaction of poly(vinyl alcohol) wit boric acid. Polymer 29:336–340
35. Wu KYA, Wisecarver KD (1992) Cell immobilization using PVA crosslinked with boric acid. Biotechnol Bioeng 39:447–449
36. Li ZQ, Hou LD, Li Z, Zheng W, Li L (2013) Study on shape optimization of calcium-alginate beads. Adv Mater Res 648:125–130